ZAMORZAEV, A. M. (1976). *The Theory of Simple and Multiple Antisymmetry.* Kishinev: Shtiintsa.
ZAMORZAEV, A. M., GALYARSKIJ, E. I. & PALISTRANT, A. F. (1978). *Colored Symmetry, its Generalizations and Applications.* Kishinev: Shtiintsa.
ZAMORZAEV, A. M., KARPOVA, YU. S., LUNGU, A. P. & PALISTRANT, A. F. (1986). *P Symmetry and its Further Development.* Kishinev: Shtiintsa.
ZAMORZAEV, A. M. & PALISTRANT, A. F. (1980). *Z. Kristallogr.* **151**, 231-248.

Acta Cryst. (1992). A**48**, 328-335

A Pentagonal Quasiperiodic Tiling with Fractal Acceptance Domain

BY E. ZOBETZ

Institut für Mineralogie, Kristallographie und Strukturchemie, Technische Universität Wien, Getreidemarkt 9, A-1060 Vienna, Austria

(*Received* 31 *May* 1991; *accepted* 22 *November* 1991)

Abstract

The structural properties of a pentagonal quasiperiodic tiling obtained by new deflation and matching rules are described. Two new types of vertices occur that cannot be found in generalized Penrose patterns. Tile and vertex frequencies as well as average edge valencies of vertices are enumerated. The geometry underlying the acceptance domain involves self-similar fractals. Two methods of constructing the fractally shaped acceptance domain have been found.

1. Introduction

Considerable progress has been made on quasiperiodic structures during the last few years. Most of the work was focused on original (Penrose, 1974, 1979; Gardner, 1977; de Bruijn, 1981; Mackay, 1982; Levine & Steinhardt, 1986; Socolar & Steinhardt, 1986; Henley, 1986; Jarić, 1986; Kumar, Sahoo & Athithan, 1986; Socolar, 1989) and generalized Penrose tilings (Duneau & Katz, 1985; Pavlovitch & Kléman, 1987; Ishihara & Yamamoto, 1988; Whittaker & Whittaker, 1988; Zobetz & Preisinger, 1990). This is not surprising since there exists a large number of tools with which to analyze them: matching and deflation rules (Penrose, 1974; Gardner, 1977; de Bruijn, 1981; Levine & Steinhardt, 1986; Socolar & Steinhardt, 1986; Socolar, 1989), grid construction methods (de Bruijn, 1981; Gähler & Rhyner, 1986; Levine & Steinhardt, 1986; Socolar & Steinhardt, 1986; Korepin, Gähler & Rhyner, 1988; Socolar, 1989) and strip-projection methods (de Bruijn, 1981; Kramer, 1982; Kramer & Neri, 1984; Duneau & Katz, 1985; Elser, 1986; Ostlund & Wright, 1986; Jarić, 1986; Kramer & Zeidler, 1989; Socolar, 1989).

Although one has to keep in mind that for any given orientational symmetry it is possible to construct an infinite number of quasiperiodic tilings that can be grouped into LI* classes (Levine & Steinhardt, 1986; Socolar & Steinhardt, 1986; Socolar, 1989), comparatively little attention has been paid to other pentagonal tilings (Gähler & Rhyner, 1986; Socolar & Steinhardt, 1986; Olami & Kléman, 1989) than original and generalized Penrose tilings. There is no reason to exclude *a priori* other tilings. Up to now we have no reason to suggest that properties of original Penrose tilings, such as matching rules, which force nonperiodicity, have direct physical significance, in the sense that the growth probability at a given site depends only on its local neighbourhood, since only growth algorithms with short-range interactions are of physical interest (Levitov, 1988; Onada, Steinhardt, DiVincenzo & Socolar, 1988, 1989; Jarić & Ronchetti, 1989; Socolar, 1990; Olami, 1991; Ingersent & Steinhardt, 1991). However, there are few proven results in this relatively new field of investigation. Hence, one is led to the conclusion that this key problem is by no means completely settled. Socolar (1989, p. 10548) stated: 'It is worth emphasizing again that the PLI† class tilings discussed in this paper, though they play a special role in the analysis of the symmetries of interest here, are not necessarily privileged candidates for modeling physical structures. It is possible that a different LI class would be required for the description of a given physical material.' Therefore tilings that have the same orientational symmetry and tile shapes as Penrose tilings, but clearly have very different local and global configurations of tiles, may also be of interest and relevance to the study of quasicrystalline materials. Baake, Schlottmann & Jarvis (1991) introduced the new equivalence concept of mutual local derivability. They prove that under special conditions a tiling can

* Two tilings are locally isomorphic and belong to the same local isomorphism (LI) class if any finite region that occurs in one also occurs in the other.

† PLI denotes the LI class of the original Penrose tilings.

0108-7673/92/030328-08$03.00

always be seen as a decoration of another suitable tiling (*e.g.* suitable decoration of the original Penrose tiling yields the kite-and-dart pattern and *vice versa*). Though these tilings do not belong to the same LI class, since they have different sets of tile shapes and different local and global configurations, they belong to the same 'equivalence' class. Therefore, this concept seems to be a further step to an exhaustive classification of quasicrystals.

By means of simple deflation rules, two new kinds of pentagonal quasiperiodic tilings with new and interesting properties have been found. Deflation procedures allow a fast, direct and unique generation of nonperiodic structures. A deflation rule is a self-similarity transformation in which each tile of the pattern can be subdivided into tiles scaled by a constant factor μ^{-1} to form a new pattern. A 'simple deflation rule' (Socolar, 1989) means that every tile of a given shape is subdivided in the same way. In the case described in this paper, $\mu = \tau^2$, where $\tau = (\sqrt{5}+1)/2$. The deflation rules have been chosen such that corners of rhombi meeting at a vertex have interior angles of either $\pi/5$ and $3\pi/5$ or $2\pi/5$ and $4\pi/5$, respectively. As a consequence, the acceptance domains (ADs) consist of only three two-dimensional planes, whereas ADs of original and generalized Penrose tilings consist of four and five planes, respectively. Both new tilings have only pentagonal average symmetry, but the tiling that will be discussed in detail in this paper also has finite regions of tenfold symmetry. The other tiling will be discussed in a forthcoming paper. The most remarkable property of both tilings is the fractal shape of their ADs.

2. Matching and deflation rules

The tiling described in this paper consists of two kinds of rhombi (Fig. 1*a*) - a large one, *RL*, with acute angle $2\pi/5$ and a small one, *RS*, with acute angle $\pi/5$. The edge length of both rhombi is *a*. Two edges of each rhombus are labelled by a + sign, the remaining two by a − sign. Corners where two edges with a + sign converge are assigned a + sign. The opposite corner has a − sign. The labelling of the edges completely determines the labelling of the vertices and *vice versa*. Corners at a pole have interior angles of $\pi/5$ and $3\pi/5$; the unmarked corners have interior angles of $2\pi/5$ and $4\pi/5$. The matching condition for these marked tiles is that edges and corners with a + sign must fit against edges and corners with a − sign. This matching rule is not a forcing rule, since one is able to tile the plane in a periodic way by means of the two rhombi. Therefore the two rhombi do not define an aperiodic set in the sense given by Grünbaum & Shepard (1987).

Fig. 1(*b*) shows how deflation can be applied to large and small rhombi. The deflation types RL_1 and RL_2 and RS_1 and RS_2, respectively, do not differ in the geometrical arrangement of their parts after one stage of deflation, but do differ after two stages. The deflated tiles can be combined to give two different types of tiling: (1) RL_1 and RS_1; (2) RL_2 and RS_2. The tiling of type 2 will be discussed in this paper.

By repeating the deflation process several times we obtain arbitrarily large patches of tiles, which implies that the whole plane can be tiled. Fig. 2 shows a patch of the tiling of type 2.

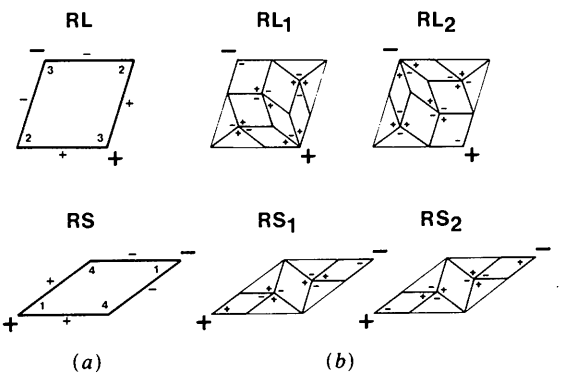

Fig. 1. Large (*RL*) and small (*RS*) rhombi. (*a*) + and − signs represent the matching rules. Edges and corners with a + sign must fit against edges and corners with a − sign. The corner angles are indicated in units of $\pi/5$. (*b*) Deflation of the rhombi with a scale factor $\mu = \tau^2$. RL_2 and RS_2 yield the tiling discussed in this paper.

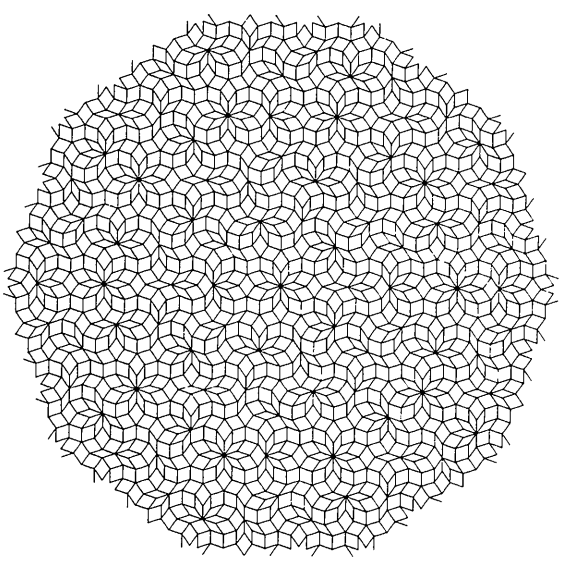

Fig. 2. A patch of the tiling by the rhombi RL_2 and RS_2. The initial stage was an ST vertex. The figure shows the innermost part of the tiling that has been obtained by repeating the deflation process three times. Five steps of deflating an *L*1 or *L*2 vertex or four steps of deflating an *N* or *P* vertex would have yielded the same result.

3. Vertex frequencies

The tiling of type 2 has seven kinds of vertex, which are denoted by Q, K, L, S, N, P and ST (Fig. 3). Q, K, S, L and ST vertices may also be found in generalized Penrose patterns (Zobetz & Preisinger, 1990). N and P are new vertices. A distinction may be made between two kinds of L vertices, namely $L1$ and $L2$, since their transformation by deflation is different. For $L1$ vertices the small rhombus has its negative end at the vertex, for $L2$ vertices it is the positive end. The deflation of an $L1$ vertex, which becomes an N vertex in the deflated tiling, and the deflation of an $L2$ vertex, which becomes a P vertex, is shown in Fig. 4. Two edges of the $L2$ vertex generate Q vertices, the remaining two generate K vertices. All four edges of the $L1$ vertex generate K vertices. The surrounding three large rhombi generate six Q, six $L1$ and three $L2$ vertices, the small rhombus one $L1$ and one $L2$ vertex. Since the vertex valency of an edge and a rhombus is 2 and 4, respectively, the number of new vertices generated on an edge must be multiplied by 1/2, that in a rhombus by 1/4.

Let $(N_Q)_n$, $(N_K)_n$, $(N_S)_n$, ... denote the number of Q, K, S, ... vertices, where n represents the stage of deflation. The substitution of vertices upon deflation can be expressed by means of a matrix $\mathbf{M}$ (Mandelbrot, Gefen, Aharony & Peyrière, 1985; Levine & Steinhardt, 1986; Kumar, Sahoo & Athithan, 1986; Olami & Kléman, 1989):

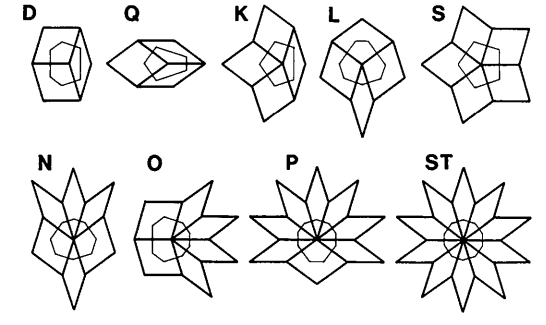

Fig. 3. Types of vertices and Voronoi polygons occurring in the tilings described in this paper. D, Q, K, L, S and ST vertices may also be found in original and generalized Penrose tilings.

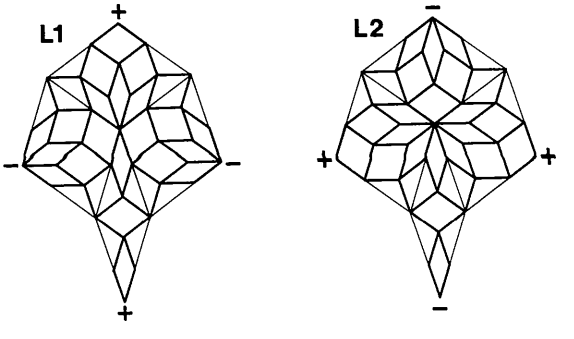

Fig. 4. Deflation of an $L1$ and an $L2$ vertex. $L1$ becomes an N vertex, $L2$ a P vertex after one stage of deflation. Two edges of the $L1$ vertex generate Q vertices, the remaining two edges K vertices. All the four edges of the $L2$ vertex generate K vertices. The adjacent three RL generate six Q, six $L1$ and three $L2$ vertices, RS generates one $L1$ and one $L2$ vertex.

Table 1. *Vertex frequencies of the tilings PT_n and DT_n corresponding to the fractal growth of the pentagonal and decagonal AD*

The subscript n denotes the stage of fractal development. FT denotes the tiling with the fractal shaped AD. The last row gives the average edge valency of vertices. The vertex frequencies of PT tilings converge to the values of FT. The vertex frequencies of DT tilings remain constant throughout the fractal development after the second stage.

Vertex	PT_0	PT_1	PT_2	PT_3	DT_0	DT_1	DT_2	FT
D	0.1230	0.0157	0.0023	0.0003	-	-	-	-
Q	0.3220	0.3017	0.2932	0.2920	0.3416	0.2918	0.2918	0.2918
K	0.1230	0.1610	0.1776	0.1799	0.0807	0.1803	0.1803	0.1803
L	0.2985	0.3743	0.3809	0.3818	0.3974	0.3820	0.3820	0.3820
$L1$	-	-	-	-	-	-	-	0.2361
$L2$	-	-	-	-	-	-	-	0.1459
S	0.0890	0.0877	0.0817	0.0808	0.1305	0.0807	0.0807	0.0807
N	0.0179	0.254	0.0323	0.341	-	0.0290	0.0344	0.0344
O	-	-	-	-	0.0190	-	-	-
P	0.0166	0.0254	0.0236	0.0216	0.0059	0.0322	0.0213	0.0213
ST	0.0099	0.0087	0.0085	0.0094	0.0249	0.0041	0.0095	0.0095
Average edge valency	3.8060	3.9752	3.9964	3.9995	4.0000	4.0000	4.0000	4.0000

$$\begin{bmatrix}(N_Q)_{n+1}\\(N_K)_{n+1}\\(N_{L1})_{n+1}\\(N_{L2})_{n+1}\\(N_S)_{n+1}\\(N_N)_{n+1}\\(N_P)_{n+1}\\(N_{ST})_{n+1}\end{bmatrix}=\begin{bmatrix}\frac{3}{2}&2&\frac{3}{2}&\frac{5}{2}&\frac{5}{2}&4&\frac{9}{2}&5\\\frac{1}{2}&\frac{3}{2}&2&1&\frac{5}{2}&-&-&-\\1&\frac{7}{4}&\frac{7}{4}&\frac{7}{4}&\frac{5}{2}&2&\frac{9}{4}&\frac{5}{2}\\\frac{3}{4}&1&1&1&\frac{5}{4}&\frac{3}{2}&2&\frac{5}{2}\\1&1&-&-&1&-&-&-\\-&-&1&-&-&-&-&-\\-&-&-&1&-&-&-&-\\-&-&-&-&-&1&1&1\end{bmatrix}\begin{bmatrix}(N_Q)_n\\(N_K)_n\\(N_{L1})_n\\(N_{L2})_n\\(N_S)_n\\(N_N)_n\\(N_P)_n\\(N_{ST})_n\end{bmatrix}.$$

The characteristic polynomial is

$$\det(\mathbf{M}-\lambda\mathbf{I})=\lambda^8-7.75\lambda^7+5.125\lambda^6+6.75\lambda^5+1.5\lambda^4-0.375\lambda^3.$$

The following eigenvalues have been calculated:

$$\lambda_1=\tau^4,\quad \lambda_2=1.5998,\quad \lambda_3=\tau^{-4},$$
$$\lambda_4=-0.4249+0.3559i,$$
$$\lambda_5=-0.4249-0.3559i,\quad \lambda_6=\lambda_7=\lambda_8=0.$$

The vertex frequencies for the infinite tiling ($n=\infty$) are given by the components x of the eigenvector $\mathbf{x}$ of the maximal eigenvalue (Mandelbrot, Gefen, Aharony & Peyrière, 1985; Olami & Kléman, 1989) (Table 1). Solution of $(\mathbf{M}-\lambda_1\mathbf{I})\mathbf{x}=0$ yields

$$\mathbf{x}=\{\sigma[10-6\tau, 10\tau-6, \tau^{-3}, \tau^{-4}, (4\tau-6)/(3\tau+1), \tau^{-7}, \tau^{-8}, 1/(\tau^7+\tau^9)]\}$$

where σ is real.

4. Determination of the acceptance domain

The projection formalism is the most powerful method to compute the diffraction patterns of quasicrystals by means of the Fourier transform of the AD (Levine & Steinhardt, 1984; Duneau & Katz, 1985; Elser 1986; Jarić, 1986). It will be briefly discused here. Consider a regular periodic hyperlattice in n-dimensional space with an m-dimensional ($m<n$) hypersurface embedded in it. Project all points that lie within a certain distance, w, from the hypersurface (the window function) onto a subspace R^m ($\mathbf{V}_E$: external, parallel or physical space). The corresponding AD is the set of all projections on R^{n-m} ($\mathbf{V}_I$: internal, perpendicular or pseudo space) of the lattice points that project onto R^m. $n=5$ for pentagonal quasicrystals of dimension $m=2$. The explicit coordinates of a lattice point $\mathbf{k}$ in R^5 with coordinates k_0, k_1, k_2, k_3, k_4 projected onto $\mathbf{V}_E$ and $\mathbf{V}_I$ are

$$\mathbf{k}_E = (\tfrac{2}{5})^{1/2}\left(\sum_j k_j \cos 2\pi j/5, \sum_j k_j \sin 2\pi j/5\right)$$

and

$$\mathbf{k}_I = (\tfrac{2}{5})^{1/2}\left(\sum_j k_j \cos 4\pi j/5, \sum_j k_j \sin 4\pi j/5, \sum_j k_j/\sqrt{2}\right),$$

respectively. All the projected lattice points in $\mathbf{V}_I$ are on planes perpendicular to the third axis, with separation $1/\sqrt{5}$. The AD of original Penrose tilings consists of four planes, those of general Penrose tilings of five planes. In our case it consists of three planes, since $\sum_j k_j$ takes only three values, say, -1, 0 and $+1$. In the case of quasicrystals, the AD is densely and uniformly filled by projected points $\mathbf{k}_I$ (de Bruijn, 1981; Elser, 1986), which implies that the frequencies of different types of vertices are proportional to the corresponding disjoint areas in $\mathbf{V}_I$. This method can be used to calculate the occurrence of the different vertices in tilings that cannot be constructed by means of deflation procedures.

A numerical approach was used to determine the shape of the AD. The projected lattice points $\mathbf{k}_I$ in $\mathbf{V}_I$ of about 50 000 vertices $\mathbf{k}_E$, generated in $\mathbf{V}_E$ by means of the deflation procedure, have been computed. The three planes of the AD, two of which, namely those corresponding to $\sum_j k_j = -1$ and $\sum_j k_j = 0$, are depicted in Fig. 5, show fivefold symmetry and are neither simple nor convex polygons. The underlying geometry is obviously not made of straight lines. The deflation process implies self-similarity relations on the shape of the AD and the disjoint areas corresponding to different types of vertices. For example, all $L1$ vertices become N vertices, and all N vertices become ST vertices after each stage of deflation, which implies that the area occupied by $L1$ vertices projected onto $\mathbf{V}_I$ is of the same shape as the area occupied by N vertices, except for the scale factor $1/\mu$ and a rotation of 180°. Comparable self-similar relations exist for the other types of vertices. Therefore, the AD was suspected to involve self-similar

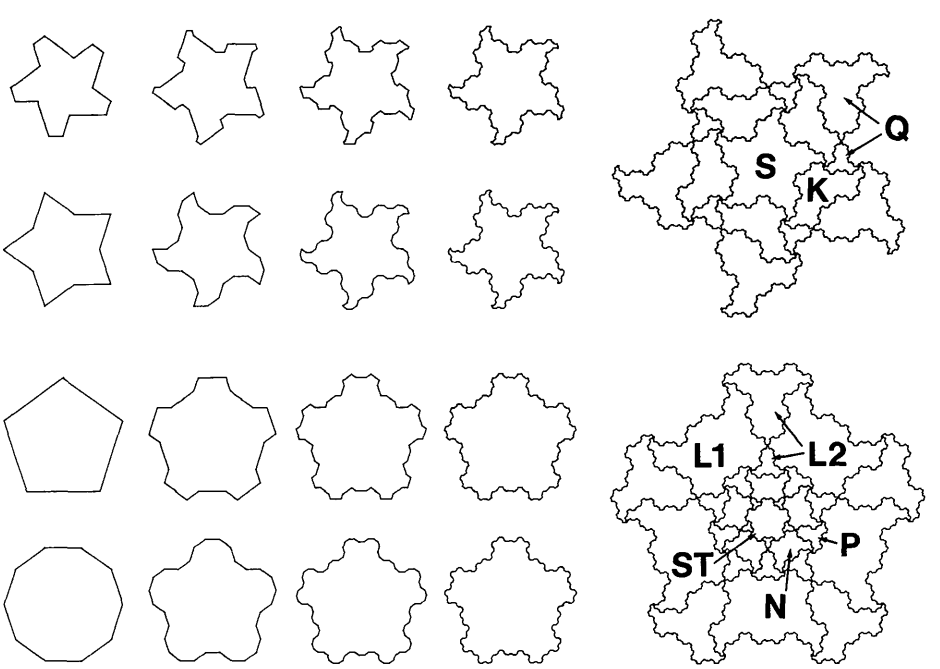

Fig. 5. The first four stages of the fractal growth of the AD. First row: $\sum_j k_j = -1$ plane, pentagonal initiator. Second row: $\sum_j k_j = -1$ plane, decagonal initiator. Third row: $\sum_j k_j = 0$ plane, pentagonal initiator. Fourth row: $\sum_j k_j = 0$ plane, decagonal initiator. The two figures on a larger scale show approximations of the fractal-shaped AD and the division into subregions corresponding to the different types of vertices.

fractals, since the underlying geometry is obviously not made of straight lines and is self-similar, but I have found no definite proof beyond these heuristic arguments.

5. Fractal development of the acceptance domain

Before we proceed with details concerning the construction of the fractal AD, let us focus on the construction of exact fractals. Many fractals - or at least their finite approximations - can also be thought of as seqences of primitive elements, for instance line segments. They are graphical objects defined in terms of rewriting rules, which usually can be carried out recursively. Mandelbrot (1983) restates the construction of the classic and well known von Koch curve (von Koch, 1905): 'One begins with two shapes, an initiator and a generator. The latter is an oriented broken line made up of N equal sides of length r. Thus each stage of the construction begins with a broken line and involves replacing each straight interval with a copy of the generator, reduced and displaced so as to have to have the same end points as those of the interval being replaced.'

Two methods of constructing the AD in the plane $\sum_j k_j = 0$ have been found. The initiator of the first method is a regular pentagon (Fig. 5), each side of length $2(\frac{2}{5})^{1/2}$ being divided into two line segments of equal length. The generator is such that it consists of $N = 3$ equal intervals with length $r = \tau^{-2}(\frac{2}{5})^{1/2}$ and the angles between the first and second legs and the second and third legs are 108 and 144°, respectively. If the generator is oriented such that the first and second line segments come to lie inside the actual initiator, the initiating line segment is called I_j, otherwise O_j. The subscripts denote the decagonal directions

$$e_j = [\cos(\pi j/5), \sin(\pi j/5)], \quad j = 0, \ldots, 9$$

and it is understood that the subscripts are taken modulo 10. Associated with each O_j and I_j is a substitution rule:

$$O_j (j = 2n) \rightarrow O_{j+9}, O_{j+1}, I_j;$$
$$O_j (j = 2n+1) \rightarrow I_{j+5}, O_{j+4}, O_{j+6};$$
$$I_j (j = 2n) \rightarrow I_{j+1}, I_{j+9}, O_j;$$
$$I_j (j = 2n+1) \rightarrow O_{j+5}, I_{j+6}, I_{j+4}.$$

The initiating regular pentagon is defined by the sequence $O_0, O_5, O_2, O_7, O_4, O_9, O_6, O_1, O_8, O_3$. The third row in Fig. 5 shows the first four stages of the development of the AD in the plane $\sum_j k_j = 0$, when starting with a regular pentagon.

The initiator of the second construction method is a regular decagon with side length $= (\frac{2}{5})^{1/2}$. Now, the generator is such that the angles between the first and second and the second and third legs are both 144°. I_j and O_j have the same meaning as above , but we need new substitution rules:

$$O_j \rightarrow O_{j+9}, I_j, O_{j+1};$$
$$I_j \rightarrow I_{j+1}, O_j, I_{j+9}.$$

The starting sequence of the regular decagon is $I_0, O_1, I_2, O_3, I_4, O_5, I_6, O_7, I_8, O_9$. The first four stages of the fractal growth of the AD in the plane $\sum_j k_j = 0$, when starting with a regular decagon, are shown in the fourth row of Fig. 5.

The development of the AD in the plane $\sum_j k_j = -1$ corresponding to both construction methods is shown in the first and second rows of Fig. 5. The last column in Fig. 5 shows approximations of the fractal shapes and the division into subregions corresponding to the different types of vertex on a larger scale. Since the AD in the plane $\sum_j k_j = 1$ is only the mirror image of that with $\sum_j k_j = -1$, it is not shown in Fig. 5.

The fractal dimension D (Madelbrot, 1983) of an exact fractal curve is defined by the equation $D = (\log N)/\log[(\frac{2}{5})^{1/2}/r]$. Since for both construction methods $N = 3$ and $r = \tau^{-2}(\frac{2}{5})^{1/2}$, we get $D = (\log 3)/(\log \tau^2) \simeq 1.1415$.

Evidence for the equivalence of the two fractal ADs is given in the Appendix.

6. Tilings corresponding to the fractal growth of the acceptance domain

Tilings corresponding to different stages of the fractal growth of the pentagonal and decagonal AD will be denoted PT_n and DT_n, respectively, where n represents the stage of fractal development. The tilings have been obtained in the following way. An edge between two vertices in $\mathbf{V}_I$ appears only when both corresponding points in $\mathbf{V}_E$ fall simultaneously onto the AD. So, starting from any point of the AD, one has to see whether the projection on $\mathbf{V}_I$ of an adjacent vertex falls inside the AD. This method to obtain a tiling is relatively simple when the number of line segments surrounding the AD is small, but is obviously a tedious and time-consuming task for tilings with complex ADs, as is the case for PTs and DTs after a particular stage of fractal development. In the case of PT_0 (Fig. 6), the starting point was chosen in the centre of the AD in the plane $\sum_j k_j = 0$, so that the tiling shows global fivefold symmetry. The AD of PT_0 in the planes $\sum_j k_j = -1$ and $\sum_j k_j = 0$ is shown on the left of Fig. 5 in the first and third row, respectively. The PTs consist of the two Penrose rhombi, an irregular octagon and a regular decagon. Two new types of vertices, N and P, occur (Fig. 3), which cannot be found in generalized Penrose tilings. The frequency of the different types of vertex for the first four stages calculated following the method described in § 4 is given in Table 1.

During the fractal growth of the AD, the frequency of the D vertices, as well as that of the octagons and decagons, decreases and converges to 0. In PT_0 the edge valency (e.v.) of the vertices (the average number of edges meeting at a vertex) is e.v. = 3.8060 (Table 1), which is significantly less than 4. This is due to the relatively large number of octagons and decagons. The edge valency is 4 if the plane tiling is entirely made of rhombi and is metrically balanced (Grünbaum & Shepard, 1987). As the fractal character of the AD grows, the average edge valency of the vertices increases and converges to 4 (Table 1).

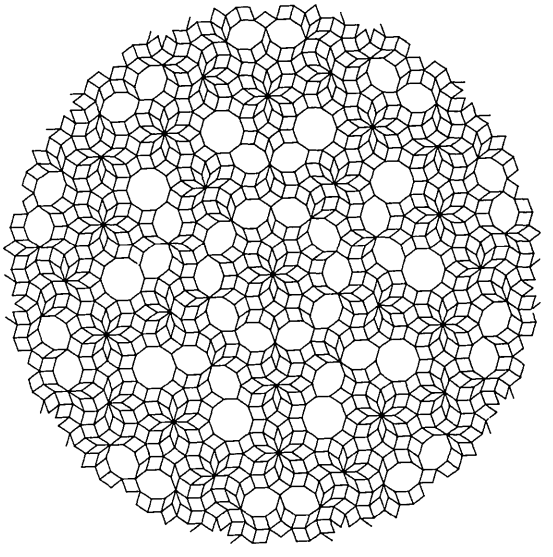

Fig. 6. A patch of PT_0 (initiating stage of the fractal growth of the pentagonal AD). Four different tiles occur in this pattern: the two Penrose rhombi *RL* and *RS*, an irregular octagon and a regular decagon.

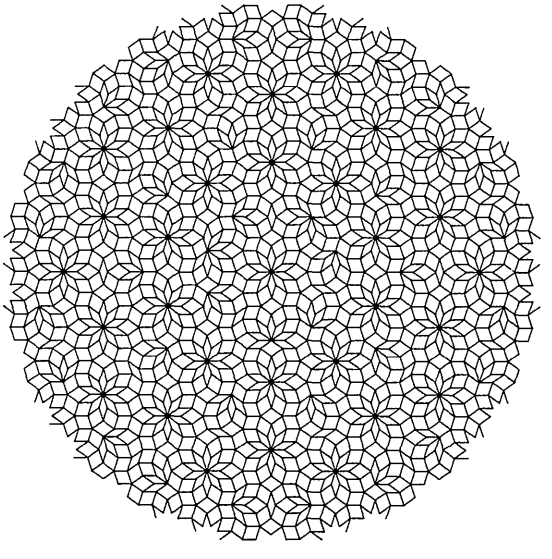

Fig. 7. A patch of DT_0 (initiating stage of the fractal growth of the decagonal AD).

In the case of DT_0 (Fig. 7), the starting point was not chosen in the centre of the AD in the plane $\sum_j k_j = 0$, but very near to it, since there exist no regular tilings (de Bruijn, 1981) with global fivefold or even mirror symmetry.* The AD of DT_0 in the planes $\sum_j k_j = -1$ and $\sum_j k_j = 0$ is shown on the left of Fig. 5 in the second and fourth row, respectively. This tiling is a slight but distinctive modification of the tiling described by Olami & Kléman (1989). The shapes of their AD are a pentagonal star, which is identical to the AD in the plane $\sum_j k_j = -1$, a large decagon (identical to the AD in the plane $\sum_j k_j = 0$) and a small decagon in the plane $\sum_j k_j = +1$. The small decagon may be obtained by omitting the areas corresponding to the Q and K vertices. Olami & Kléman (1989) derived their AD using a Voronoi construction in $\mathbf{V}_I$ to maximize the packing fraction in $\mathbf{V}_E$ (Olami & Alexander, 1988). In the tiling with the complete AD there occur seven types of vertex, Q, K, L, S, N, O and ST (Fig. 3). The frequency of occurrence of the different types of vertex and the edge valency of the vertices for the first three stages of fractal development are listed in Table 1. The vertex frequencies have been calculated as described in § 4. It is an interesting feature of these tilings that, after the second stage of fractal growth, the vertex frequencies representing the first coordination sphere remain constant and it seems plausible that, depending on the fractal stage, this will be also true for higher coordination spheres.

The fractal growth of the AD, whose limit is the fractal AD, is characterized by decreasing-size approximations. Increasingly small peninsulas and bays are added to and squeezed in the AD *ad infinitum*. The decreasing-size approximations can also be seen in the corresponding tilings. If one erases all Q, K and L vertices of a DT_{n+1} tiling, one obtains a DT_n tiling with larger rhombi, scaled by a factor τ^2. The area of the S, N, P and ST vertices of DT_{n+1} in $\mathbf{V}_\parallel$ has the same shape as the AD of the DT_n tiling, reduced by a factor τ^{-2}. If one starts from the same generic point, the intersection $AD_{n1} \cap AD_{n2}$ of two different ADs yields the acceptance domain AD_{n12} of a tiling, whose vertices can be found in both DT_{n1} and DT_{n2}. The ratio of the area of AD_{n12} to AD_{n1} may serve as a measure of agreement between the two tilings (Table 2).

Since $\sum_j k_j$ takes only the values -1, 0 and $+1$, it can easily be seen that rhombi can only be decomposed in the way depicted in Fig. 1. Inversion of inflated *RS* does not change the position of any vertex, but inversion of inflated *RL* changes the

* If one starts for instance with an ST vertex in the centre of the AD, then the process of projection does not lead to an unambiguous tiling, since there will be points $\mathbf{k}_I$ that will fall on the boundary of adjacent vertices. Here, we exclude any consideration of singular tilings.

Table 2. *The agreement between two tilings AD_{n1} and AD_{n2}*

The ratio of the area of intersection of two ADs to the area $\sum_i A_i$, which remains constant throughout the fractal growth, serves as a measure of agreement between two different tilings. $\sum_i A_{n12i}$ is the area of the intersection $AD_{n1} \cap AD_{n2}$ of two different ADs. $n1$ and $n2$ ($n2 > n1$) denote different stages of fractal development. The fraction of coinciding vertices, FCV, is given by $\sum_i A_{n12i}/\sum_i A_i$, with $\sum_i A_{n12i} = \sum_i A_i - 3^{n1+1}(3-\tau)(\sin \pi/5)/\tau^{4n1+2}$, and $\sum_i A_i = (2\tau+4)\sin(2\pi/5)$. Since $\sum_j k_j$ takes only the values -1, 0 and $+1$, inflated rhombi can only be decomposed as shown in Fig. 1. Inversion of inflated *RL* changes the position of three vertices. The fraction of inflated *RL*, FIIRL, that has to be inverted to obtain complete coincidence is given by $(1-\text{FCV})(8\pi+5)/3$.

$n1$	FCV (%)	FIIRL (%)
0	86.4745	50.0000
1	94.0800	21.8847
2	97.4088	9.5788
3	98.8659	4.1926
4	99.5036	1.8351
5	99.7827	0.8032
6	99.9049	0.3516
7	99.9584	0.1539
8	99.9818	0.0673
9	99.9920	0.0295
10	99.9965	0.0129
15	99.999944	0.000207
20	99.99999910	0.00000333

position of three vertices. Therefore, the fraction of inflated *RL* that has to be inverted to yield a tiling of any of the subsequent stages may also serve as a measure of agreement between two tilings (Table 2).

7. A quasiperiodic tiling by fractal tiles

The fractal shapes of the subregions of the AD corresponding to the different types of vertices can be used to tile the plane in a nonperiodic way. One example is shown in Fig. 8. The deflation of the three fractal tiles corresponding to the vertices ST, *P* (*Q*, *L2*), and *N* (*L1*) is shown in Fig. 8(*b*). The following substitution matrix may be established:

$$\begin{bmatrix} (N_{ST})_{n+1} \\ (N_P)_{n+1} \\ (N_N)_{n+1} \end{bmatrix} = \begin{bmatrix} 1 & 1 & 1 \\ 5 & 3 & 4 \\ 5 & 1 & 3 \end{bmatrix} \begin{bmatrix} (N_{ST})_n \\ (N_P)_n \\ (N_N)_n \end{bmatrix},$$

where (N_{ST}), (N_P) and (N_N) denote the number of ST, *P* and *N* tiles, respectively. The subscripts denote the stage of deflation. The eigenvector of the maximal eigenvalue $\lambda_1 = \tau^4$ yields

$$(N_{ST})_\infty : (N_P)_\infty : (N_N)_\infty = 5-3\tau : 7-4\tau : 7\tau-11.$$

The eigenvector of the maximal eigenvalue of the transposed matrix yields the ratio of the areas of the three tiles

$$(A_{ST})_\infty : (A_P)_\infty : (A_N)_\infty = 2\tau-1 : 1 : \tau.$$

Fig. 8(*a*) shows an *ST* tile after two steps of deflation. The fractal shape of the tiles does not force nonperiodicity as can be seen in Fig. 9, where a patch of a periodic tiling by *N* and *P* tiles is shown.

8. Concluding remarks

There is a seemingly unlimited variety of quasiperiodic tilings belonging to different LI classes, which may be generated by choosing new deflation and/or matching rules, generalized grid methods and window functions or ADs, which are the sets of projected points in $\mathbf{V}_I$ of the *n*-dimensional lattice

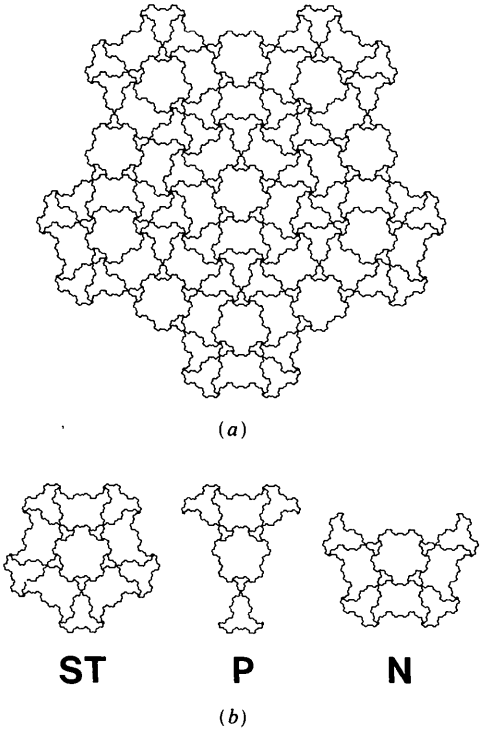

(*a*)

(*b*)

Fig. 8. Quasiperiodic pentagonal fractal tiling. The fractal tiles correspond to the regions marked ST, *P* and *N* in Fig. 5. (*a*) An ST tile after two stages of deflation. (*b*) Deflation of the fractal tiles ST, *P* and *N*.

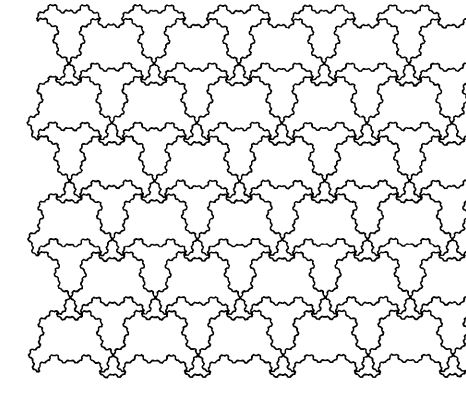

Fig. 9. A patch of a periodic tiling by fractal *N* and *P* tiles.

points defined by the window function. Derivation of the Fourier transforms of fractal ADs, even of finite approximations, will be a tedious task and the calculation of numerical values will be time consuming. Moreover, there exists an unlimited number of quasiperiodic tilings, generated by deflation rules with a scale factor $\mu = \tau^{2n}$ (some of these with $\mu = \tau^2$ and $\mu = \tau^4$ will be described in a forthcoming paper), whose fractal ADs also consist of three planes and look very similar, at least at first glance, but have very different local and global configurations. This again raises the question of to what extent it is possible to determine the real structure of a quasicrystal, although very promising results in the structure determination have been obtained (*e.g.* Steurer & Kuo, 1990; Steurer, 1991). However, one has to keep in mind that most structure determinations were carried out employing *ad hoc* assumptions about the window functions (Fibonacci crystals: bars; octagonal quasicrystals: regular octagons; decagonal quasicrystals: regular pentagons and decagons).

The author thanks one of the referees for constructive comments on the manuscript and for pointing out relevant references.

APPENDIX

Arguments supporting the claim of equivalence of the fractal ADs generated by means of the pentagonal and decagonal AD construction methods are as follows.

(1) Both ADs are fractal, have the same fractal dimension and consist of only three planes ($\sum_j k_j = -1, 0, +1$).

(2) The area of both ADs and the frequency of vertices converge to the same values. The area $\sum_i A_i^n = (2\tau+4)\sin(2\pi/5) \simeq 6.8819$ (A_i^n is the area of the $\sum_j k_j = i$ plane of the AD and n denotes the stage of development) of the DT_n ADs remains constant throughout the fractal development. The number of added peninsulas is the same as the number of bays that are squeezed in at every stage. Both peninsula and bay have the same shape and area P_n, where $P_n = \sin(2\pi/5)/5\tau^{4n}$. The area of the initiating pentagonal AD is given by $\sum_i A_i^0 = 3/(\sin 2\pi/5) + (4\tau+8)(\sin 2\pi/5)/5 \simeq 5.9072$, which is significantly less than 6.8819. The area of 30 peninsulas P_n is added at each stage. Each addition of 30 increasingly small peninsulas increases the area of the AD,

$$\sum_i A_i^n = \sum_i A_i^0 + 6(\sin 2\pi/5) \sum_{j=1}^{n} \tau^{-4j}.$$

Hence, the value of the area of the fractal-shaped AD,

$$\sum_i A_i^\infty = \sum_i A_i^0 + 6(\sin 2\pi/5) \sum_{j=1}^{\infty} \tau^{-4j},$$

is easily seen to be just the area of the decagonal fractal-shaped AD [$\sum_{j=1}^{n} \tau^{-4j}$ converges to $(\tau^4-1)^{-1}$ for $n=\infty$]. Comparable equations exist for the disjoint areas corresponding to the different types of vertices and confirm that the vertex frequencies converge to the values derived by means of the substitution matrix **M** for the tiling of type 2 (Table 1).

(3) Most convincing, though not a justification, is the fractal development of both ADs shown in Fig. 5.

References

BAAKE, M., SCHLOTTMANN, M. & JARVIS, P. D. (1991). *J. Phys. A*, **24**, 4637-4654.

BRUIJN, N. G. DE (1981). *Proc. K. Ned. Akad. Wet. Ser. A*, **43**, 39-52, 53-66.

DUNEAU, M. & KATZ, A. (1985). *Phys. Rev. Lett.* **54**, 2688-2691.

ELSER, V. (1986). *Acta Cryst.* A**42**, 36-43.

GÄHLER, F. & RHYNER, J. (1986). *J. Phys. A*, **19**, 267-277.

GARDNER, M. (1977). *Sci. Am.* **236**, 110-121.

GRÜNBAUM, B. & SHEPARD, G. C. (1987). *Tilings and Patterns.* New York: Freeman.

HENLEY, C. L. (1986). *Phys. Rev. B*, **34**, 797-816.

INGERSENT, K. & STEINHARDT, P. J. (1991). *Phys. Rev. Lett.* **64**, 2034-2037.

ISHIHARA, K. N. & YAMAMOTO, A. (1988). *Acta Cryst.* A**44**, 508-516.

JARIĆ, M. V. (1986). *Phys. Rev. B*, **34**, 4685-4698.

JARIĆ, M. V. & RONCHETTI, M. (1989). *Phys. Rev. Lett.* **62**, 1209.

KOCH, H. VON (1905). *Acta Math.* **30**, 145-174.

KOREPIN, V. E., GÄHLER, F. & RHYNER, J. (1988). *Acta Cryst.* A**44**, 667-672.

KRAMER, P. (1982). *Acta Cryst.* A**38**, 257-264.

KRAMER, P. & NERI, R. (1984). *Acta Cryst.* A**40**, 580-587.

KRAMER, P. & ZEIDLER, D. (1989). *Acta Cryst.* A**45**, 524-533.

KUMAR, V., SAHOO, D. & ATHITHAN, G. (1986). *Phys. Rev. B*, **34**, 6924-6932.

LEVINE, D. & STEINHARDT, P. J. (1984). *Phys. Rev. Lett.* **53**, 2477-2480.

LEVINE, D. & STEINHARDT, P. J. (1986). *Phys. Rev. B*, **34**, 596-616.

LEVITOV, L. S. (1988). *Commun. Math. Phys.* **119**, 627-666.

MACKAY, A. L. (1982). *Physica (Utrecht)*, A**114**, 609-613.

MANDELBROT, B. B. (1983). *The Fractal Geometry of Nature.* New York: Freeman.

MANDELBROT, B. B., GEFEN, Y., AHARONY, A. & PEYRIÈRE, J. (1985). *J. Phys. A*, **18**, 335-354.

OLAMI, Z. (1991). *J. Phys. I*, **1**, 43-62.

OLAMI, Z. & ALEXANDER, S. (1988). *Phys. Rev. B*, **37**, 3973-3978.

OLAMI, Z. & KLÉMAN, M. (1989). *J. Phys. (Paris)*, **50**, 19-33.

ONADA, G. Y., STEINHARDT, P. J., DIVINCENZO, D. P. & SOCOLAR, J. E. S. (1988). *Phys. Rev. Lett.* **60**, 2653-2656.

ONADA, G. Y., STEINHARDT, P. J., DIVINCENZO, D. P. & SOCOLAR, J. E. S. (1989). *Phys. Rev. Lett.* **60**, 1210.

OSTLUND, S. & WRIGHT, D. C. (1986). *Phys. Rev. Lett.* **56**, 2068-2071.

PAVLOVITCH, A. & KLÉMAN, M. (1987). *J. Phys. A*, **20**, 687-702.

PENROSE, R. (1974). *Bull. Inst. Math. Its Appl.* **10**, 266-271.

PENROSE, R. (1979). *Math. Intell.* **2**, 32-37.

SOCOLAR, J. E. S. (1989). *Phys. Rev. B*, **39**, 10519-10551.

SOCOLAR, J. E. S. (1990). *Commun. Math. Phys.* **129**, 599-619.

SOCOLAR, J. E. S. & STEINHARDT, P. J. (1986). *Phys. Rev. B*, **34**, 617-647.

STEURER, W. (1991). *J. Phys. Condens. Matter*, **3**, 3397-3410.

STEURER, W. & KUO, K. H. (1990). *Acta Cryst.* B**46**, 703-712.

WHITTAKER, E. J. W. & WHITTAKER, R. M. (1988). *Acta Cryst.* A**44**, 105-112.

ZOBETZ, E. & PREISINGER, A. (1990). *Acta Cryst.* A**46**, 962-969.